Soft Matter

PAPER

View Article Online
View Journal

Cite this: DOI: 10.1039/d5sm01147g

The effect of molecular shape and chemical structure on the photo-physical properties of liquid crystals

Jordan Hobbs, [a] Richard J. Mandle, [ab] Johan Mattsson [a] and Mamatha Nagaraj *[a]

Fluorescence in liquid crystals (LCs) is valuable for applications such as optoelectronic devices, photovoltaics and light emitting diodes. The molecular shape and chemical structure of LCs greatly influence their fluorescent properties, although these relationships are not well understood. We here provide a systematic comparative study of a selection of cyanobiphenyl-based LCs with both calamitic and dimeric molecular shapes. The influence of both these molecular shapes and of lateral fluorination on the observed fluorescence is determined. Our results show that cyanobiphenyl-based calamitic nematic LCs exhibit a constant increase in the excimer-to-monomer emission ratio as the temperature is reduced from the isotropic phase. For a cyanobiphenyl-based dimeric LC with an average bent (or banana) molecular shape, that exhibits both nematic and twist-bend nematic phases, the excimer-to-monomer ratio is found to be constant within both the isotropic and the nematic phases. However, interestingly, a significant increase in the excimer-to-monomer ratio is observed in the lower temperature twist-bend nematic phase of this material, indicating an increased presence of anti-parallel (AP) pairing modes. When the same dimeric LC is fluorinated laterally to the cyano group, the material shows significantly less excimer emission compared to the non-fluorinated dimeric LCs due to an interruption in AP pairing. Furthermore, the results on cyanobiphenyl-based LCs are compared with results for an oxadiazole-based nematic bent-core LC that does not support the same AP pairing modes. For the oxadiazole-based LC, we observe a constant excimer-to-monomer ratio that is significantly smaller compared with that observed for the other LCs throughout the entire temperature-range of the nematic phase. Our results clearly demonstrate that the fluorescence of cyanobiphenyl-based LCs, directly linked to excimer formation, is almost exclusively a result of AP pair formation. Importantly, we also demonstrate that this pair formation, and thus the fluorescence, can be tuned both through modification of the molecular shape and chemical structure.

Received 15th November 2025,
Accepted 9th January 2026

DOI: 10.1039/d5sm01147g

rsc.li/soft-matter-journal

1 Introduction

Fluorescent liquid crystals (LCs) are highly desirable for a wide variety of potential applications including polarised lasers,[1,2] displays,[3–5] organic light emitting diodes (OLEDs),[6,7] photonic devices,[8,9] ink-jet print dyes[10] and 1-D semiconductors.[11] Their desirability stems from the ability to tune their photo-physical properties *via* application of an external electric field, or by tuning of the interfacial (surface) conditions. The study of the emission properties of LCs in their neat form is essential for their use in emission-driven device applications. However, LCs' fluorescent properties are often investigated only in dilute solution. Although LCs can be highly fluorescent in solution, once they are concentrated their behaviours typically change, either due to the molecular arrangements imposed by the concentration-driven phase change, or simply due to intermolecular interactions and related effects, such as excimer formation.[12] Even when the emission properties of LCs are studied in their neat form, many studies are often incomplete. Generally the study of fluorescence of neat LCs are performed on 'bulk' LC samples within cuvettes to enable compatibility with measurements performed using a 'standard' set-up. However, cuvette measurements are not representative of LC-based device applications, which require that the LCs are used in sandwich-cells or specific devices. The cuvette geometry also requires additional care in the interpretation of the data due to their significant optical density. Thus, it is best to avoid the use of cuvette geometries for measurements on neat LC samples.[13]

[a] School of Physics and Astronomy, University of Leeds, Leeds, UK.
E-mail: M.Nagaraj@leeds.ac.uk
[b] School of Chemistry, University of Leeds, Leeds, UK

In LCs, excimer emission can strongly affect the fluorescence properties. An excimer is a molecular complex formed between the ground-state and the excited-state of the same molecular species. Excimers are unstable, and will therefore decay either through fluorescence, also known as excimer emission,[12,14] or through a non-radiative process; both routes act to quench the emission output of the monomer.[15,16] Excimer formation can both red-shift and alter the emission spectra or even lead to a complete quenching of the fluorescence[17] and various applications have been developed, which utilise excimer formation and emission.[18–20] Excimer emission is generally red-shifted compared to the ground state emission, since the excimer occupies a lower energy state compared to that of the corresponding monomer. Excimer formation is diffusion-activated (*i.e.* it requires close molecular proximity and is thus dependent on diffusion for these encounters) and so is influenced both by the temperature and viscosity of the material.[21] Klock *et al.* postulated that the formation of fluorescent excimers (in both dilute solutions of LCs in solvent, as well as in neat LCs) is related to the antiparallel (AP) pair formation in these materials.

Excimer formation has been previously investigated in some calamitic LCs, such as alkyl- and alkoxy-cyanobiphenyls (*n*CB and *n*OCB).[13,22–30] It has been found that when *n*CB or *n*OCB is dissolved in an isotropic solvent at low concentrations (<100 mM although generally the limit is solvent-dependent), the observed fluorescence emission is blue-shifted and predominantly corresponds to monomer emission. As the LC-concentration in the isotropic solvent was significantly increased, a red-shifted emission was observed, suggesting the formation of dimers or excimers.[13,23,24] In fact, it is now well-known that *n*CB or *n*OCB LCs show AP pair formation, where individual mesogens pack top-to-tail,[31–34] and such AP pair formation has been observed in both the nematic and isotropic phases.[35,36] Klock *et al.* proposed three different possible AP excimer conformations for *n*CB and *n*OCB LCs; these conformations are termed fully-overlapped, partially-overlapped and twisted-charge-transfer conformations.[26] From X-ray diffraction analysis of the dimer length,[34] and from time-resolved fluorescence measurements on a bridged version of 9CB (that prevents the formation of a twisted conformation[26]) it was shown that the dominant excimer form in *n*CB and *n*OCBs is the fully overlapped AP dimer. Based on investigations of neat nematic LCs, it was suggested that the excimer formation is assisted by the orientational order of the nematic phase.[22,24,25] Time-resolved fluorescence spectroscopy studies have also shown that excimer formation, while possibly enhanced by the nematic phase, is still present in the isotropic phase.[25] It has also been suggested that excimer emission could possibly occur both from dimers formed pre- and post-excitation.[24]

Calamitic LCs show a relatively limited conformational flexibility and this restricts the excimer formation to nearest-neighbour interactions, which typically means that a smaller degree of local order is required for significant AP-pair interactions. On the other hand, bent-core mesogens, and banana-shaped molecules, can have either rigid or flexible central cores[37–40] and can thus experience a variety of intermolecular interactions, which might significantly affect the excimer formation. In the past, the emission properties of bent-core LCs have been studied mostly in dilute solutions, where any effects due to the formation of the LC phase are not observed.[41–44] For bent-core LCs, investigated in their LC phases, it has been found that similar to the behaviour of other anisotropic materials, they demonstrate both absorption and emission anisotropy,[44,45] as well as excimer emission.[44,46] It is important to note, however, that often the reported results include data acquired using a cuvette geometry, and does not capture the complete picture.[13]

This paper provides a systematic comparative study of the fluorescence properties of a selection of LCs, carefully chosen to identify the role of molecular shape as well as structural modifications to their photo-physical properties. All investigated LCs are investigated in their neat form, within sandwich devices, using a front-face geometry.[13] The paper is divided into three parts. The first part contains a detailed investigation of the photo-physical properties of two cyanobiphenyl LCs: 5CB, which exhibits a nematic phase, and 8CB, which exhibits both a nematic and a smectic A phase, respectively. In the second part, the results for a cyanobiphenyl-based LC dimer (containing CB monomeric units), characterised by a mesogen with a bent 'banana' shape is investigated. The dimer contains the same fluorescent moiety as the investigated corresponding calamitic LCs (5CB/8CB) allowing the specific study on molecular shape. The effect of fluorination on AP formation is also investigated, for a dimeric nematic LC based on the same cyanobiphenyl dimer. In the third part of the paper, the results from all four cyanobiphenyl type LCs are compared with an oxadiazole-based nematic bent-core LC that does not allow any AP pair formation. Our results demonstrate how the photo-physical properties of LCs can be tuned by variation of molecular shape and specific fluorination *via* manipulation of anti-parallel interactions.

2 Materials and methods

The LCs used in this work are: 4-(4-pentylphenyl)benzonitrile (5CB), 4-(4-pentylphenyl)benzonitrile (8CB), 4-[4-[7-[4-(4-cyanophenyl)phenyl]heptyl]phenyl]benzonitrile (CB7CB), 4-[4-[7-[4-(4-cyanophenyl)phenyl]heptyl]phenyl]benzonitrile (F-CB7CB) and 4-(5-(4-((4-(dodecyloxy)benzoyl)oxy)phenyl)-1,3,4-oxadiazol-2-yl)phenyl 4-pentylbenzoate (VBG93). The chemical structures, phase sequence and phase transition temperatures of these materials are provided in Fig. 1. F-CB7CB (synthesis details given in SI) shows monotropic N and N_{TB} phases; F-CB7CB transitions to the N phase at 48.5 °C and to the N_{TB} phase at 41 °C. This significant decrease in T_{NI} compared to CB7CB is consistent with the trend observed for fluorinated *n*CBs,[47] where disruption of the AP packing by fluorination destabilizes the LC phases and reduces the T_{NI} significantly. VBG93, used in this paper, was re-synthesised according to Görtz *et al.*[48] 5CB

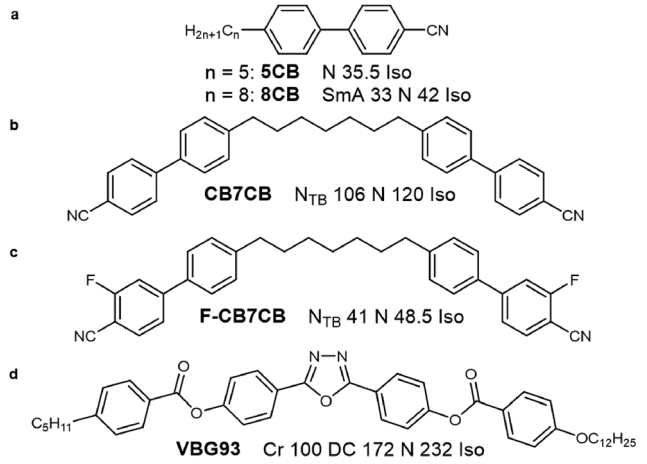

Fig. 1 Molecular structure, phase sequence and phase transition temperatures of the liquid crystals used in this paper. (a) For 5CB and 8CB where n = 5, 8 respectively, (b) CB7CB, (c) F-CB7CB and (d) VBG93. Phase transitions were determined from changes in polarised optical microscopy texture. Iso: isotropic, N: nematic, N_{TB}: twist-bend nematic, DC: dark conglomerate and Cr: crystal.

and 8CB were purchased from Sigma Aldrich and CB7CB from Synthon, and these were used without further purification. All LCs used here showed significant supercooling of their LC phases, allowing for data collection far below their nominal crystallisation temperatures. The planar and homeotropic LC cells were purchased from AWAT, Poland. Planar alignment in the liquid crystal cells was achieved using a SE130 polyimide alignment layer and the substrates were rubbed and assembled anti-parallel. The homeotropic alignment was achieved using a SE1211 polyimide alignment layer. All LC cells had a cell gap of 10 μm and, unless mentioned, were filled in the nematic phase. The alignment quality, and phase transitions, were determined using polarised optical microscope (POM) and differential scanning calorimetry (DSC). DSC experiments were performed using a TA Instruments Q20 heat flux DSC in combination with a liquid nitrogen cooling system.

Fluorescence spectroscopy was carried out using a fluorescence spectrometer (Edinburgh Instruments FLS1000) equipped with dual monochromators. An ozone-free xenon arc lamp was used to excite the samples using unpolarised light, which was directed *via* optical fibres to a Linkam hot-stage. For a planar sample, the excitation and subsequent emission collection were normal to the LC director, and in a homeotropic sample they were parallel to the director. As mentioned in the introduction, compared to measurements in cuvettes, measurements in cells significantly reduce spectral distortions resulting from primary and secondary inner-filter effects.[49,50] More details on the setup used for LC materials is discussed elsewhere.[13] All emission measurements were corrected for the specific optics of the entire setup.

The temperatures of the LCs were controlled using a Linkam T95 temperature controller equipped with a LST120 Peltier stage for the experiments on 5CB, 8CB and F-CB7CB, and a Linkam THMS600 stage for CB7CB and VBG93. Emission spectra were recorded using excitation and emission bandwidths of 1 nm except for VBG93 for which a 2 nm bandwidth was used due to the low fluorescence emission of the material. An excitation wavelength of 310 nm for 5CB, 8CB and CB7CB, a wavelength of 335 nm for F-CB7CB, and 330 nm for VBG93 was used. Emission spectra were measured on cooling using a rate of 1 °C min^{-1}, except for F-CB7CB for which a cooling rate of 5 °C min^{-1} was used due to the tendency of the sample to crystallise under slow cooling. The spectra of an empty LC cell, mounted on a hotplate, was subtracted from the LC spectral data prior to the analysis, to remove any background effects. The background spectra showed a slight temperature dependence and background spectra were hence collected at all the relevant temperatures.

Spectrometers used in fluorimetry generally measure the photon count per wavelength. However, to fit the emission data using a Gaussian-type peak, it is important to convert the data from a wavelength (λ) scale to a wavenumber (ν) scale to account for the inhomogeneous broadening that occurs on the energy scale.[51] In this paper, the abscissa was converted using

$$\nu = \frac{1}{\lambda}. \tag{1}$$

The ordinate, in-turn, requires the use of the Jacobian conversion,[52,53] and the conversion used here is thus given by:

$$f(\nu) = f(\lambda)\frac{\mathrm{d}\lambda}{\mathrm{d}\nu} = -f(\lambda)\lambda^2. \tag{2}$$

We note that this conversion is essential, as evenly spaced intervals on a wavelength scale are not evenly spaced on a wavenumber scale and the data thus requires a correction for this fact. After the correction was applied, Gaussians were fitted to the emission spectra. For all LCs in this paper, a fit using two Gaussians provided the best fit, as determined by minimising the fitting residual. The equation used to fit the data is given by:

$$I = A_{\mathrm{m}}\exp\left(\frac{-4\ln(2)(\nu-\nu_{\mathrm{m}})^2}{{w_{\mathrm{m}}}^2}\right) + A_{\mathrm{e}}\exp\left(\frac{-4\ln(2)(\nu-\nu_{\mathrm{e}})^2}{{w_{\mathrm{e}}}^2}\right), \tag{3}$$

where I is the intensity, A_n the amplitude of the peak, ν_n the position of the peak, and w_n is the full width half maximum (FWHM). The subscript n corresponds to m and e for monomer and excimer emissions, respectively. For all LCs investigated in this work, the lower wavelength (higher wavenumber) peak corresponds to the monomer emission, while the higher wavelength (lower wavenumber) corresponds to the excimer emission. Fig. 2 shows such fitted curves for the 5CB liquid crystal in its isotropic phase at two different temperatures (100 °C and 60 °C). The graphs Fig. 2(a) and (b) show the emission intensity *vs.* wavenumber at the two different temperatures, illustrating both the change in the monomer and excimer contributions as the temperature was varied. The contributions from the monomer and the excimer are shown together with the cumulative fit

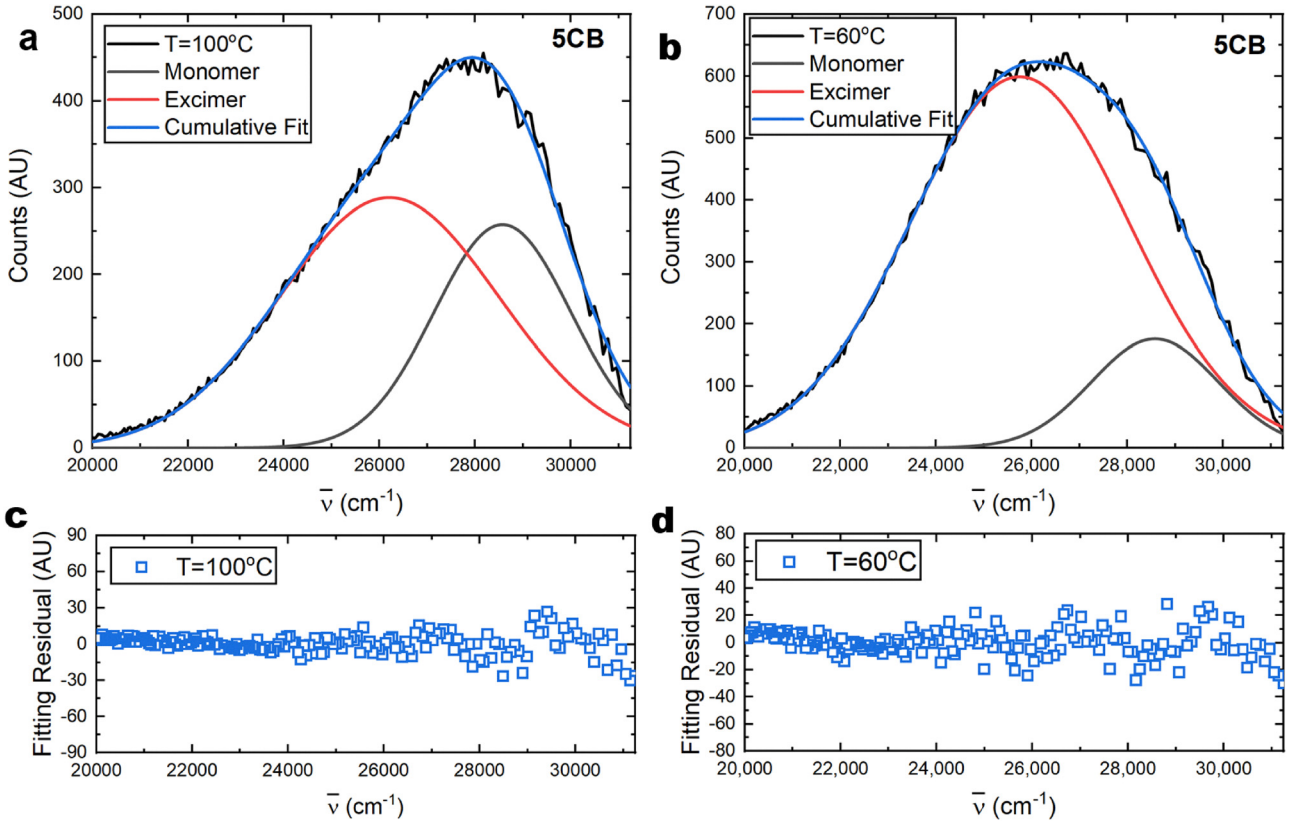

Fig. 2 Representative fit obtained for 5CB in its isotropic phase at (a) 60 °C and (b) 100 °C. Fitting residuals for the above fits are in (c) and (d). The lack of sine wave shape in the fitting residual indicates that the only difference between the fit obtained and the original data is the random noise associated with the experiment.

and the corresponding fitting residual, all as a function of wavenumber.

3 Results and discussion

3.1 Anisotropic emission from 5CB and 8CB liquid crystals

Fig. 3a and b show the emission spectra of 5CB LC in both planar and homeotropic geometries. Both datasets were recorded on cooling at equal temperature intervals between 100 °C and 0 °C. Fig. 3c shows the plot of the integrated area under the emission intensity peaks as a function of the temperature. Here, the intensity has been normalised to 1 for $T - T_{NI} = 0$ °C. Clearly, in the isotropic phase of 5CB, both planar and homeotropic samples show the same average emission intensity that, as expected, decreases for increasing temperature. Generally, a decreasing temperature increases the emission intensity, due to the increase in the quantum yield of the material arising from the decrease in competing decay pathways, such as molecular collisions or intra-molecular vibrations.[54] At $T = T_{NI}$, the intensities of both the planar and the homeotropic geometries show a step-change in emission intensity. The planar sample shows a larger step increase, whereas the homeotropic sample shows a much smaller step decrease. As the temperature is reduced further, the intensity of the emission increases more strongly in the planar sample compared to the behaviour in the homeotropic sample; in the latter, the intensity increases only very slightly. Considering the experimental geometry, in the planar aligned sample, the LC director is normal to the illumination and collection directions of the excitation source and subsequent detection.

In contrast, for the homeotropic sample the LC director is parallel to the illumination and collection directions. For a temperature just below $T = T_{NI}$, this results in an increase in the emission intensity from the planar sample and a decrease from the homeotropic sample. While the quantum yield might be affected by the longitudinal molecular ordering of the nematic phase, both homeotropic and planar aligned samples should be affected in the same way by this effect. This suggests that the emergence of an emission anisotropy in the nematic phase is not due to any changes in quantum yield, and is predominately due to the emergence of absorption anisotropy in the LC phases. We also note that changes in orientational order must affect the results for each alignment differently. For a planar geometry, an increase in the orientational order parameter $\langle P_2 \rangle$ would act to increase the emission intensity as the projection of the long molecular axis normal to the incoming light source is increased. In a homeotropic geometry the opposite is observed where increases in $\langle P_2 \rangle$ reduce the projection of the long molecular axis normal to the incoming light source and so

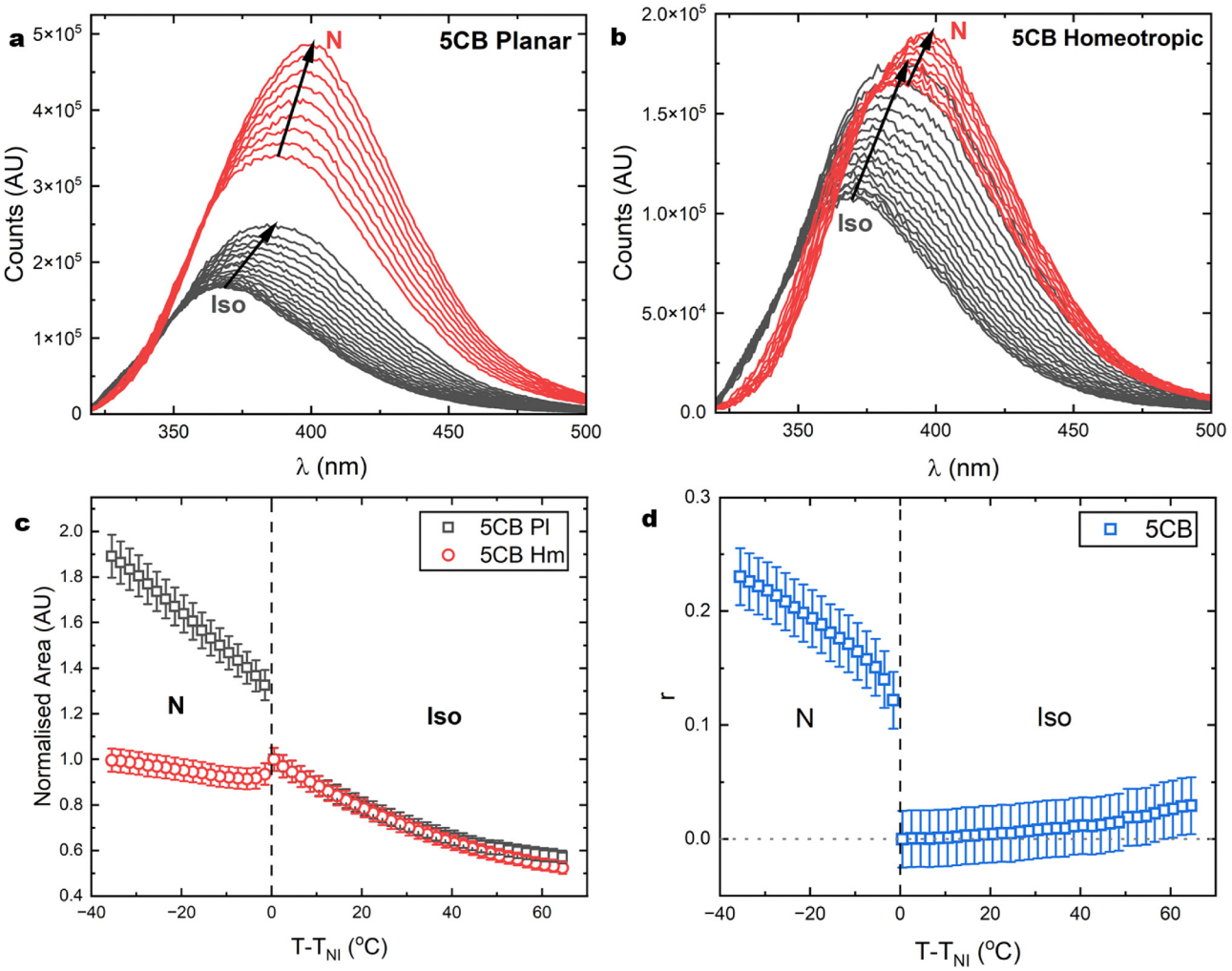

Fig. 3 The emission spectra of 5CB as function of wavelength from (a) planar and (b) homeotropic samples. The direction of the black arrows in (a) and (b) shows the direction of decreasing temperature. (c) Plot of normalised emission intensity in both planar (black squares) and homeotropic (red circules) alignments as function of temperature. It includes the emission intensity of both the isotropic and nematic phases. The data was normalised to $T - T_{NI} = 1$ for both alignments. (d) Plot of emission anisotropy obtained from (c) as function of temperature.

reduce the emission intensity. The fact that molecules oriented normal to the excitation source shows increased absorption, suggests that the $S_0 \rightarrow S_1$ transition moment is aligned with the long axis of the 5CB molecule.[55,56]

The emission anisotropy, r, is defined as:

$$r = \frac{I_\perp - I_\parallel}{I_\perp + 2I_\parallel}, \quad (4)$$

where $I_\perp$ is the emission intensity from the planar aligned cell (or absorption perpendicular to the director) and $I_\parallel$ is the emission intensity of the homeotropic cell (absorption parallel to the director). Fig. 3d shows the emission anisotropy as a function of temperature for 5CB. In the isotropic phase, r is close to zero (within error) while in the nematic phase, r increases to 0.12 immediately after the isotropic to nematic phase transition, and it increases to 0.23 by 0 °C (or $T - T_{NI} = -35.5$ °C). Across the isotropic phase, there is a slight decrease in r as the temperature is reduced. This is likely not showing an actual decrease in the anisotropy but is instead caused by photo-bleaching of the 5CB LC, or photo-degradation of the alignment layer in the cell. Photo-bleaching is not often considered to be significant for emission measurements as constant replenishment of the measurement volume reduces photo-bleaching effects, but for small sample volumes, or solid state samples, photo-bleaching can become relevant.[57] In this case the samples would begin to photo-bleach immediately resulting in an initially small change in the emission intensity. Further cooling and subsequent emission measurements leads to a steadily increasing photo-bleaching effect. Samples that are in planar alignment would experience increased photo-bleaching due to their increased absorption factor *vs.* the homeotropic LCs. The normalisation strategy used here of normalisation close to $T = T_{NI}$, attempts to mitigate this somewhat by normalising to the key region of interest; the phase transitions. This effectively shifts the discrepancies in emission intensity due to the

photo-bleaching effect to the high and low temperature limits of the axis.

Fig. 4a and b show the emission spectra of the 8CB LC as a function of wavelength, in planar and homeotropic samples. Similar to 5CB, 8CB shows an overall increase in emission intensity as the temperature was lowered. Fig. 4c and d show the evolution of emission intensity and anisotropy as a function of temperature. Both the isotropic and nematic phases of 8CB behave similarly to their 5CB counterparts, where the dominant parameter affecting the emission anisotropy is the director orientation with respect to the incoming polarization direction and the order parameter. As $\langle P_2 \rangle$ increases through the N phase, the planar aligned sample sees an increase in emission intensity and the homeotropic aligned sample shows a decrease. However in the SmA phase, both samples show an initial decrease in emission intensity before following the overall increase as the temperature was reduced. Similar to 5CB, the emission anisotropy shows a step increases at T_{NI}, due to the new longitudinal ordering, that increases throughout the N phase due to an increase in $\langle P_2 \rangle$. At T_{SmN} there is an increase in emission anisotropy due to a further increase in $\langle P_2 \rangle$ that occurs upon transition to the SmA phase.[58,59] This follows the same behaviour as the birefringence in 8CB, for which there is an increase in birefringence at T_{SmN} that is attributed to an increase in $\langle P_2 \rangle$.[58] However, for the refractive indices, n_e increases while n_o decreases at $T_{Sm\text{-}N}$, while for the emission intensity both components show a reduction in intensity. This suggests that while the emission anisotropy is dominated by the magnitude of $\langle P_2 \rangle$, the exact change in the emission intensity at $T_{Sm\text{-}N}$ has other significant contributions. The SmA phase is significantly more scattering than the N phase[60] and, in general, increased scattering has been shown to reduce the fluorescence emission.[61] Changes in the viscosity must also be considered, which will increase going from the N to SmA phase.[62] An increasing viscosity has been shown to increase emission in many fluorescent materials[63] and thus the step at the N to SmA phase is likely a superposition of changes in $\langle P_2 \rangle$, viscosity and scattering behaviour.

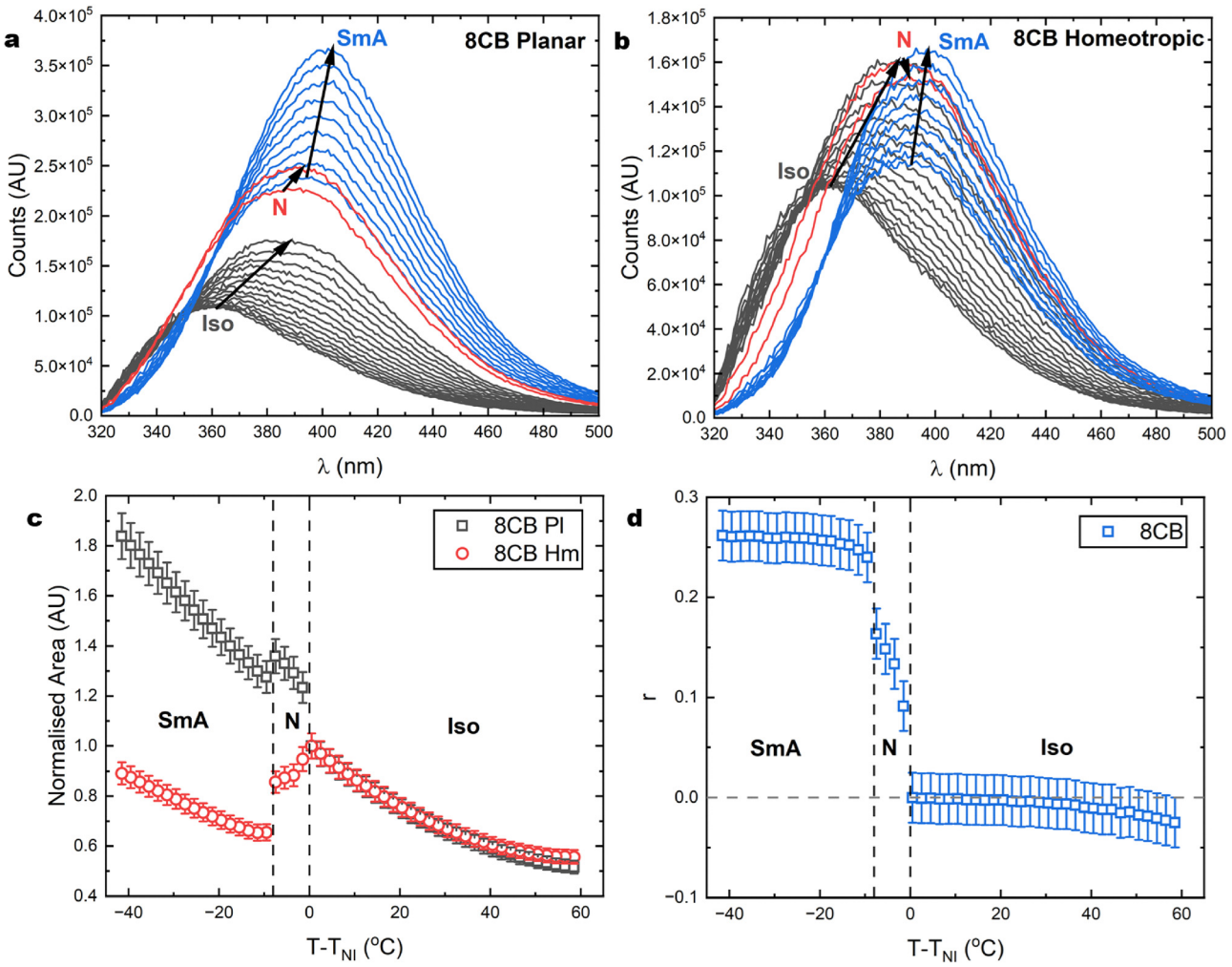

Fig. 4 Emission spectra of 8CB in (a) planar and (b) homeotropic alignment. The direction of the arrows shows the direction of decreasing temperature. Both sets of data were recorded evenly spaced between 100 °C and 0 °C. (b) Normalised emission intensity in both planar and homeotropic alignments for 8CB. The data was normalised to $T - T_{NI} = 1$ °C for both alignments. (d) Emission anisotropy for 8CB.

3.2 Excimer formation in 5CB and 8CB

The emission spectra for both 5CB and 8CB can be fitted using dual Gaussians, where the lower wavelength (higher wavenumber) Gaussian is related to monomer emission and the higher wavelength (lower wavenumber) peak is related to excimer emission. For both 5CB and 8CB, a shift in the population from monomer emission to excimer emission is seen as the temperature is decreased. This is shown in Fig. 5 where the area of each peak is plotted as a function of temperature. Both materials show a steady transfer from a combination of monomer and excimer emissions to mainly excimer emission as the temperature is decreased. In the LC phases, the gradient of the excimer emission curve is slightly higher for 8CB compared to 5CB. This is likely due to the higher order parameter of 8CB,[58,59] which may assist in the formation of AP pairs. The data shown in Fig. 5 implies that at high enough temperatures ($T - T_{NI} \sim 90$ °C) 5CB and 8CB's fluorescence emission are overwhelmingly originating from the monomer emission. This limiting temperature value is determined by extrapolating a linear fit through the isotropic excimer emission data as shown in Fig. 5a. For 5CB, this extrapolated temperature value agrees with the results found from dielectric spectroscopy studies, where at this temperature, the AP interactions are suggested to cease.[31] This suggests that the excimer emission in 5CB and 8CB is almost exclusively due to the formation of AP pairs.

3.3 Excimer formation in CB7CB

CB7CB is a flexible banana-shaped dimeric LC with the same fluorescent moiety as in 5CB and 8CB. The emission spectra, integrated area and peak position for CB7CB are shown in Fig. 6. Again, similar to 5CB and 8CB, in CB7CB, as the temperature is reduced, an increase in emission intensity and a general red-shift were observed. This suggests that for CB7CB, the formation of excimers increases as the temperature is lowered. There is also a step change at $T = T_{NI}$, as seen for 5CB and 8CB. This is not surprising since CB7CB is anisotropic and in the planar geometry will see an increase in fluorescence due to the preferential absorption along the long axis of the molecules, similar to that for 5CB and 8CB. At the N to N_{TB} transition, a step decrease in intensity is observed. Experimental results[64] and MD simulations[65] have shown that transitioning from the N to the N_{TB} phase is associated with a decrease in the nematic order parameter $\langle P_2 \rangle$ due to the heliconical tilt angle and so the reduction is likely due to an increased projection out-of-plane of the molecular cores, due to the helical N_{TB} structure, as well as a slight reduction in alignment quality.

The deconvolution of the emission spectra of CB7CB into the separate monomer and excimer peaks shows the influence of molecular shape to these contributions. As the temperature of the sample was reduced, for 5CB and 8CB, the emission peaks showed a steady shift in population from excimers to monomer. However, for CB7CB this is different. Fig. 7 shows the area of the monomer and excimer peaks for CB7CB as a function of temperature. In the Iso and N phases, the ratio of excimer-to-monomer emission remains roughly constant. The slight increase in peak area with decreasing temperature in the N and Iso phases is likely due to the fact that in general fluorescent materials have a higher quantum yield at lower temperatures due to less collision-based quenching.[66] However, in the N_{TB} phase, the ratio of excimer-to-monomer emission increases considerably due to a steady decrease in the monomer emission and an increase in excimer emission. These results indicate that the bent nature of the CB7CB molecule inhibits the transition from monomer to excimer emission even

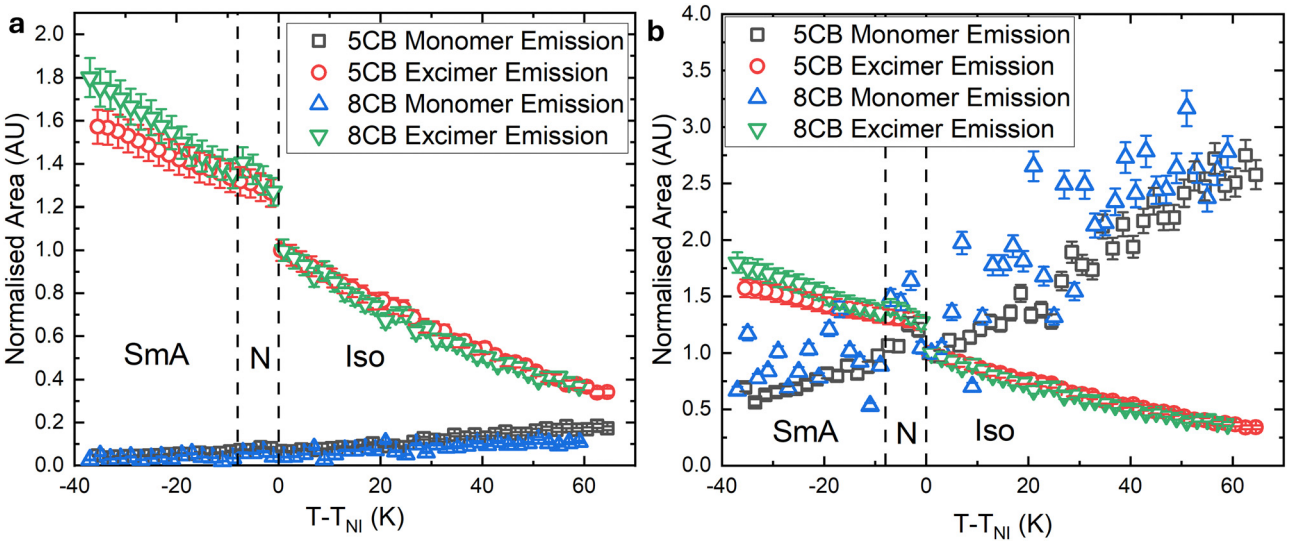

Fig. 5 Area under the Gaussian peaks for monomer and excimer emission for both 5CB and 8CB LC. Data in (a) has been normalised to the monomer intensity value at $T - T_{NI} = 1$. For (b) all data has been normalised to its own intensity value at $T - T_{NI} = 1$. The vertical line denoting the phase transition from the N to SmA phase, applies only for 8CB. The increased scatter for 8CB is due to a decreased overall emission intensity making an already weak peak harder to fit for. The decreased intensity of 8CB is an experimental effect rather than a sample effect.

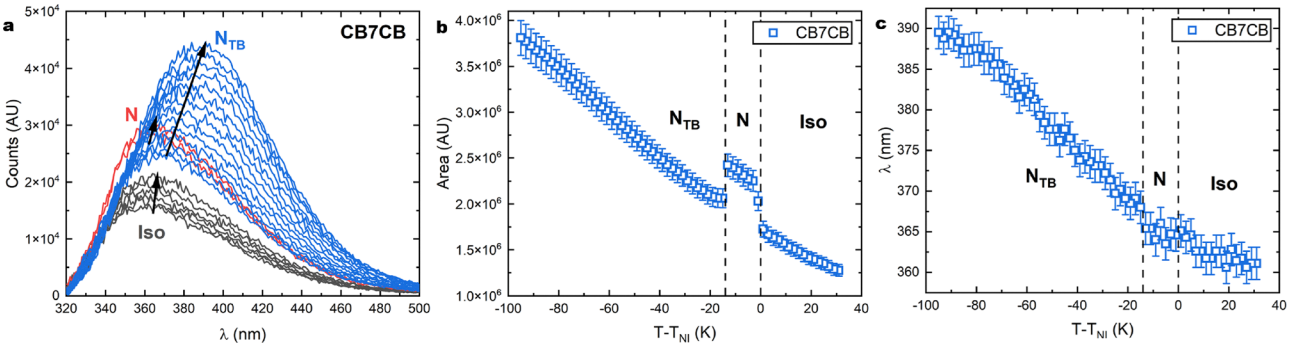

Fig. 6 (a) The emission spectra of CB7CB in the Iso, N and N_{TB} phase. Arrows indicate decreasing temperature. (b) Integrated area of the emission spectra of CB7CB as a function of temperature. Dashed vertical lines indicate phase changes. (c) The wavelength of the overall peak position (the emission wavelength) for CB7CB emission showing significant red-shifting at decreased temperatures.

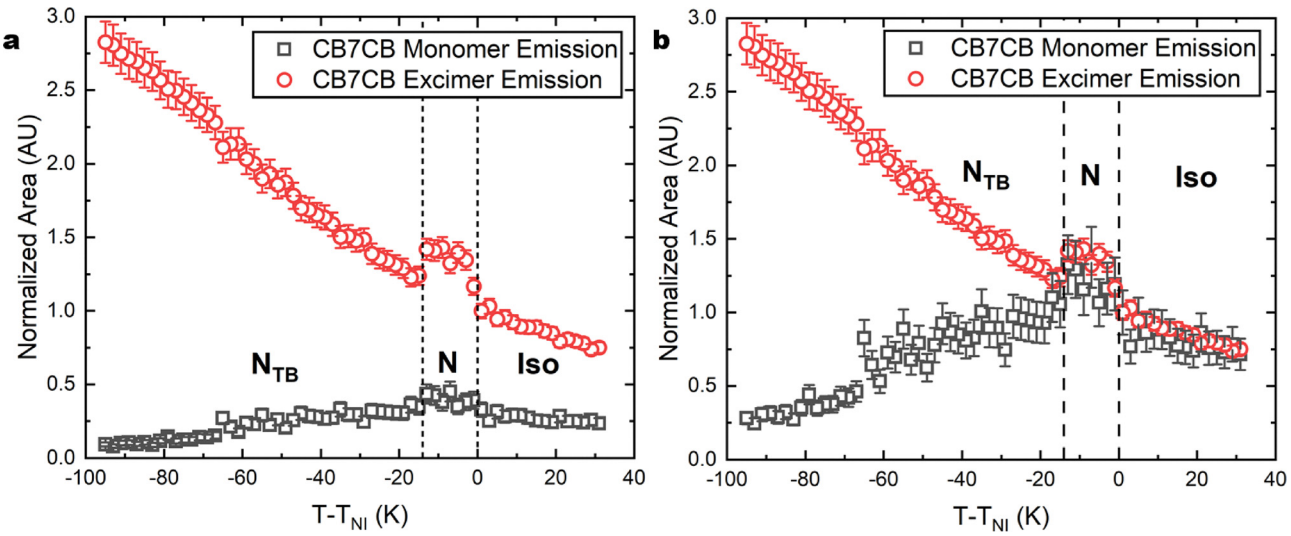

Fig. 7 Area of the gaussians used to fit for monomer and excimer emission for CB7CB. Data has been normalized to (a) excimer emission at $T - T_{NI}$ = 1 °C for both excimer and monomer emission, (b) excimer and monomer emission at $T - T_{NI}$ = 1 °C for excimer and monomer emission respectively.

though the temperature of the samples was reduced in the isotropic and nematic phases. It has been suggested that anti-parallel packing, like that for the CB-based calamitics, is highly important for the formation of the N_{TB} phase[67] where they assist in the formation of polymeric like intermolecular chains of molecules.[67,68] It has also been suggested from infra-red spectroscopy studies that for some flexible CB-based dimeric LCs, the transition into the N_{TB} phase causes an increase in the AP pair formation,[69,70] which would explain the increase in excimer emission and decrease in monomer emission throughout the N_{TB} phase, seen here. However, it is possible that it is not just the increased AP pair formation that contributes to the increased excimer formation. CB7CB has been shown to experience a shift in conformer populations in the N phase. At higher temperatures CB7CB shows predominately lower bend angle extended banana conformations while at lower temperatures the conformations are dominated by the lower bent angle hairpin conformation.[71,72] The low bend angle (30°) in the hairpin conformation[73] could be small enough that due to CB7CB's symmetric but split conjugated system, the CB7CB molecule forms excimers with itself. Intra-molecular excimer formation has been observed for a cyclodextrin dimer where biphenyl moieties form excimers with biphenyl moieties within the same molecule[74] as well as in other non-LC flexible dimer molecules,[75] though recent all-atom molecular dynamics simulations have shown that the population of hairpin molecules in the LC phases of CB7CB may not change significantly[76] which would not allow for self excimer formation to become more dominant for the N_{TB} phase than for the N.

3.4 Excimer formation in F-CB7CB

F-CB7CB is a fluorinated version of CB7CB and exhibits almost no AP pair formation. Fig. 8a shows fluorescence spectra of F-CB7CB as a function of temperature across the Iso, N and N_{TB} phases. The temperature-dependence of the change in intensity is consistent with the non-fluorinated CB7CB where there is a step increase at T_{NI} and a step decrease at the transitions from N to N_{TB}. These behaviours can be explained in the same way as

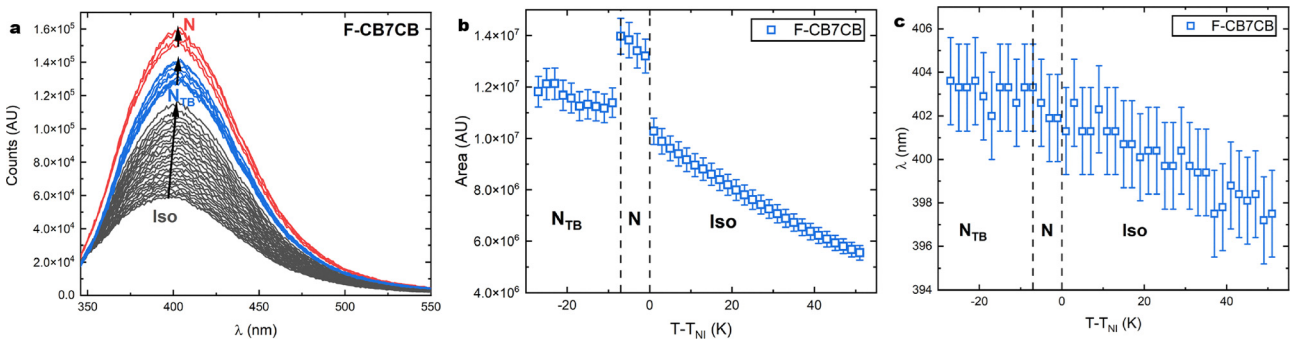

Fig. 8 (a) The emission spectra of F-CB7CB in the Iso, N and N_{TB} phase. Arrows indicate decreasing temperature. (b) Integrated area of the emission spectra of F-CB7CB as a function of temperature. (c) The wavelength of the overall peak position for CB7CB emission showing significant red-shifting at decreased temperatures. Dashed vertical lines indicate phase transitions.

the observations for CB7CB where going from the Iso to the N phase results in an increased absorption along the long axis of the molecule, in turn leading to increased emission. In the N_{TB} phase, the presence of helical twist result in some molecules becoming slightly out-of-plane with the excitation leading to reduced emission. However, there are differences in the emission spectra obtained for CB7CB *vs.* F-CB7CB. The emission wavelength of F-CB7CB is red-shifted to around 400 nm compared with around 360 nm for the Iso phase of CB7CB. The position of the peak maximum of F-CB7CB also varies only within the wavelength range between 398–404 nm, across a temperature range of 70 °C, which is a much smaller wavelength spread than that observed for CB7CB (360–390 nm) across a temperature window of 125 °C. Fluorine is strongly electronegative and has been used to significantly alter both the emission and absorption properties of some fluorophores.[77–81] Therefore, red-shifted absorption and emission spectra are not unexpected but they are noteworthy since this means that any potential F-CB7CB excimer emission would be red-shifted even further. The large red-shift of the emission spectra for CB7CB was in Section 3.3 attributed to AP pair formation. F-CB7CB, on the other hand, shows a relatively small degree of red-shifting with only a wavelength shift of 6 nm over the temperature range studied (the wavelength shift is ∼30 nm for CB7CB). This observation is indicative of a lack of AP pair formation for laterally fluorinated CB-based LCs.[47,82] We use the same spectral deconvolution approach as used for *n*CBs and CB7CB to investigate the details of the AP pair formation in F-CB7CB. Thus, the F-CB7CB spectra were deconvoluted into two separate Gaussians. Fig. 9 shows a plot of the integrated area within the monomer and excimer emission profiles as a function of temperature. From the deconvolution of the emission spectra, we find that while the excimer emission is significantly reduced by fluorination, a small amount can still be observed. The ratio of excimer-to-monomer emission follows a similar pattern to that of CB7CB, where it varies only slightly in the Iso and N phases, but then begins to sharply increase in the N_{TB} phase, due the increased AP pair formation present in this phase *vs.* in the N or Iso.

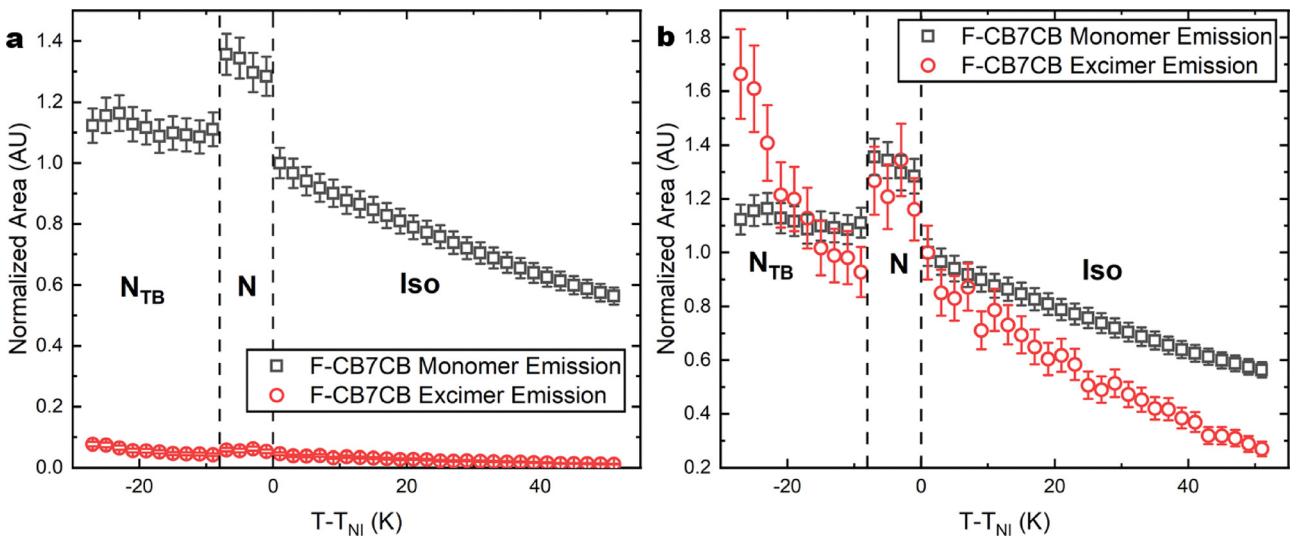

Fig. 9 Area of the gaussians used to fit for monomer and excimer emission for F-CB7CB. Data has been normalized to (a) excimer emission at $T - T_{NI} = 1$ for both excimer and monomer emission, (b) excimer and monomer emission at $T - T_{NI} = 1$ for excimer and monomer emission respectively.

3.5 Excimer formation in VBG93

VBG93 is a rigid bent-core LC that does not exhibit a N_{TB} phase; instead VBG93 has a N phase followed by a dark conglomerate (DC) phase.[83,84] The DC phase of VBG93 is comprised of two structural moieties of differing length-scales. On shorter length-scales, the phase structure is that of deformed polar smectic layers, for which the deformation appears as a wave-like modulation.[84,85] On longer length-scales, these smectic layers continuously curve such that a sponge-like structure is achieved analogous to that of a lyotropic L_3 phase.[86] Fig. 10a shows the emission spectra of VBG93 as a function of decreasing temperature through the isotropic, N and DC phases. The overall emission intensity of VBG93 is lower than the emission intensity for the CB-based LCs. Although this behaviour does lead to a decreased accuracy of the data, clear trends in the data are still observed. Fig. 10b shows the plot of overall emission intensity as function of temperature. At T_{NI}, a step increase in intensity is observed consistent with the observations for *n*CBs and CB7CB. However, at $T_{DC\text{-}N}$ a significant step decrease in the emission is observed, where the emission becomes even lower than that of the isotropic phase. The DC phase as 3D curvature and so the local director becomes optically averaged due to the large measurement volume meaning the sample effectively appears isotropic to the incoming light source. An increase in scattering of the phase *vs.* the nematic and isotropic phase results in an emission intensity lower than that of even its isotropic phase.

The results for the DC phase is also different from the results for the Iso, N and N_{TB} phases in that instead of the emission intensity increasing with decreasing temperature, the emission intensity actually decreases throughout the phase, where two regimes of different intensity *vs.* temperature gradient are observed. The temperature at which the gradients change ($T - T_{NI} = -110$ °C) is approximately the same as the temperature at which the periodicity of the smectic layer spacing increases.[83] This change is suggested to be due to the phase becoming spongier in the lower temperature regime which could increase the scattering in the and result in the reduction of the emission intensity.

Fig. 10c shows the variation of the wavelength of the emission peak with temperature. In contrast to the behaviour of the *n*CBs and CB7CB, there are only small variations in the peak wavelength throughout the Iso and N phases. A slight red-shift is observed in the DC phase, but this signifies a lack of any significant shift in the emission populations, and the emission spectra of VBG93 can be fitted using dual Gaussians accounting for monomer and excimer emission contributions; the area under each peak is shown in Fig. 11. It is noticeable that the ratio of the excimer-to-monomer emission is lower for VBG93 than for the non-fluorinated LCs presented here, and that the ratio of excimer-to-monomer emission stays $\sim$1 for the entire investigated temperature range. This demonstrates that for VBG93, LC self-assembly has no significant effect on the excimer formation. The chemical structure of VBG93 is such that almost the entire molecule is conjugated, with only breaks across the ester linkages. Side-by-side H-aggregates have been observed in the crystal phase of a flexible pyrene-CB-based LC dimer[46] and have been suggested to be present in a cyanostilbene-based bent-core LC.[41] It is possible that VBG93 forms H-aggregates in both the Iso and LC phases and that the observed excimer emission is some excimer form of the ground state H-aggregate, although this seem does unlikely due to the fact that H-aggregates are generally non-fluorescent[87,88] though some exceptions to this have been found.[89–91]

3.6 AP interactions and excimer formation

Fig. 12 shows how the ratio of excimer-to-monomer emission varies for all the materials studied. For 5CB and 8CB, the rate of transfer from monomer-to-excimer emission is approximately exponential and is independent of the Iso and N phases. Excimer formation in *n*CBs has been shown to be related to the formation of AP pairs in both the Iso, N and SmA phases,[22,24] and it has been suggested that the N phase can assist in excimer formation[25] but the results presented in Fig. 12 suggest that for the *n*CBs, AP pair formation is not significantly affected by the presence of longitudinal N type ordering and is instead a thermally activated process in the Iso and N phases. For 8CB, which exhibits a SmA phase, there

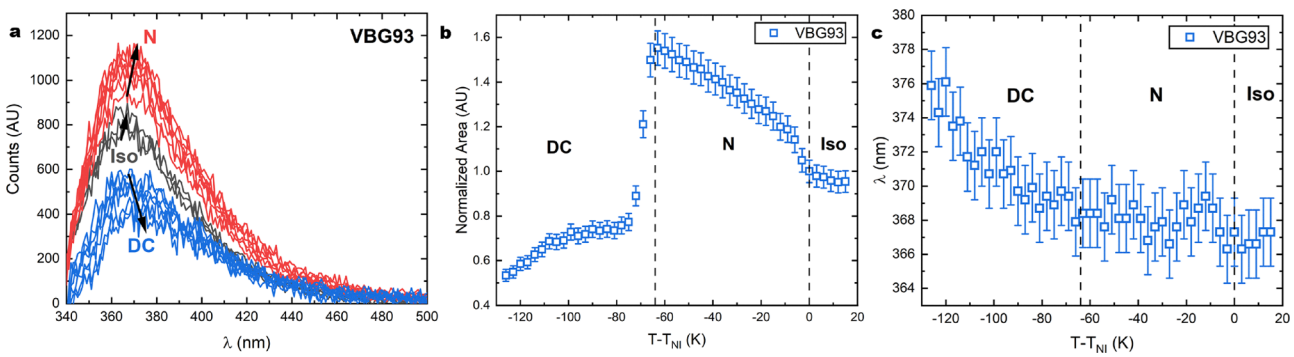

Fig. 10 (a) Emission spectra of VBG93 in the Iso, N, and DC phases. Arrows indicate decreasing temperature. (b) Integrated area of VBG93's emission spectra. The step and change in gradient in the DC phase around $T - T_{NI} = -130$ is around the same temperature at which the smectic layer spacing increases.[83] (c) The emission wavelength for VBG93 as a function of temperature. The vertical dashed lines represent the phase transition temperatures.

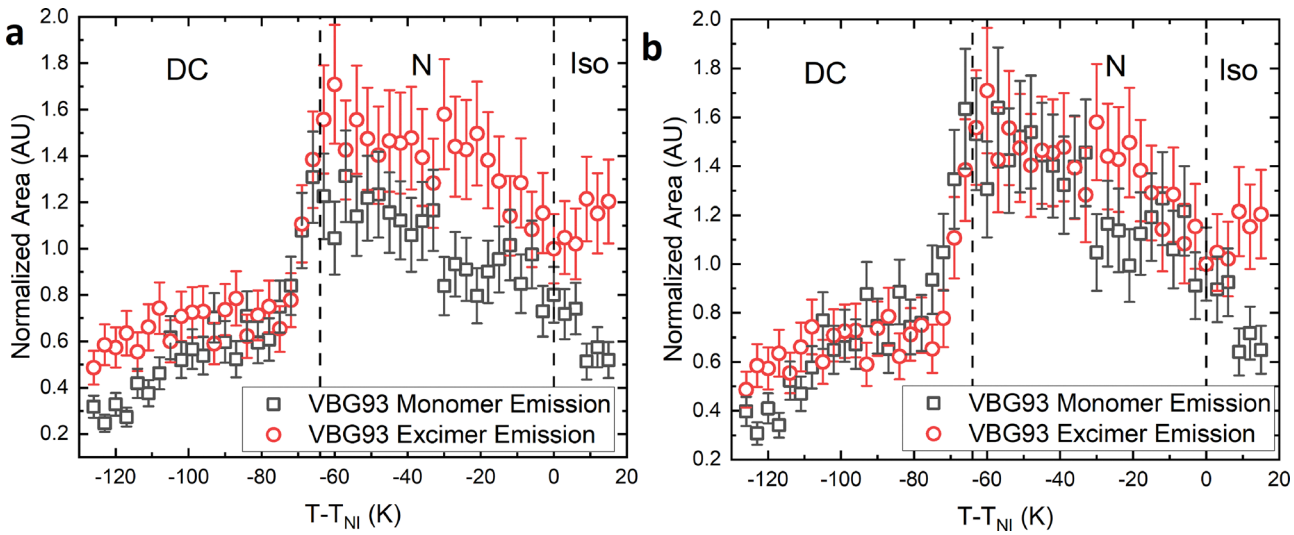

Fig. 11 Area under Gaussian peak for excimer and monomer emission for VBG93. Data has been normalized to (a) excimer emission at $T - T_{NI} = 1$ for both excimer and monomer emission, (b) excimer and monomer emission at $T - T_{NI} = 1$ for excimer and monomer emission respectively.

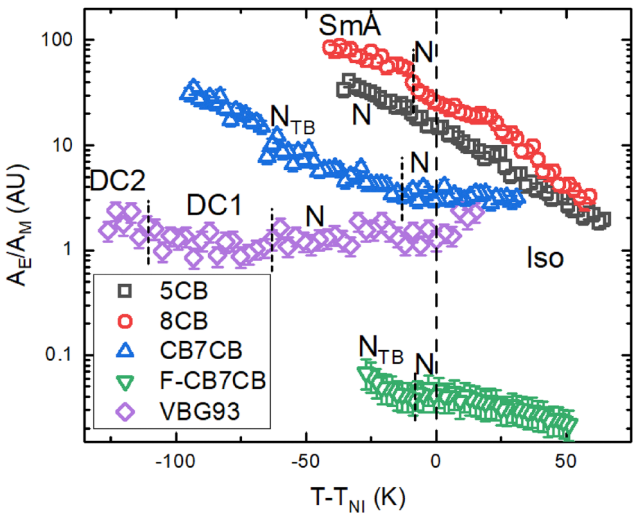

Fig. 12 The ratio of the area of excimer and monomer emission for 5CB, 8CB, CB7CB, F-CB7CB and VBG93. Dashed lines show phase transitions and adjacent labels indicate phases for the relevant material.

is an increase in A_E/A_M at $T_{Sm\text{-}N}$ due to the layer structure of the SmA phase, which is known to encourage AP interactions.[92]

For CB7CB in the Iso and N phases, the ratio of excimer-to-monomer emission remains constant at $A_E/A_M \sim 3$. Transitioning into the N_{TB} phase causes an increase in the AP pair interactions,[69,70] which subsequently causes an increase in excimer formation and thus the ratio of A_E/A_M begins to increase. The helical twist in the N_{TB} phase increases the overlap of the CB units allowing for increased AP interactions and thus more excimer emission. However the results here do not suggest an absence of AP interactions in either the N or Iso phases, just a steady increase throughout the N_{TB} phase likely due to the increasing CB overlap as suggested by Merkel *et al.*[70]

F-CB7CB shows a significantly lower value of $A_E/A_M \sim 0.04$ in the Iso and N phase compared to $A_E/A_M \sim 3$ for CB7CB. It is known that fluorination of CB-based LCs adjacent to the cyano group interrupts the AP pair formation,[47,82] leading to a significant reduction in excimer formation. From this reduction of A_E/A_M it can be concluded that excimer formation in these CB-based LCs is almost entirely related to the AP interactions. This understanding of the structure–property relationship behind excimer formation in CB-based LCs is useful for the design of fluorescent LCs that exhibit thermo-chromic behaviour controlled *via* the formation of AP excimers. This technique could be applied to other LC molecules and phases such as the ferroelectric nematic phase (N_F)[93] where parallel molecular interactions has been suggested as a key driver of the inversion symmetry breaking found in this phase.[94–96]

VBG93 consistently shows less excimer emission compared to the non-fluorinated CB-based LCs. In the CB-based LCs, the transition dipole moment is parallel to the long axis, and the timescale of rotation of this dipole is therefore significantly longer than if the dipole moment was oriented parallel to the short axis; this situation may act to increase the excimer formation efficiency. In VBG93, the transition dipole moment is along the short axis of the molecule. This means that the dipolar rotation is much faster, which increases the difficulty of excimer formation compared to the situation in the *n*CBs and in CB7CB; the flexible spacer in the CB7CB dimer allows the CB units to effectively act individually.

4 Conclusions

Fluorescence spectroscopy of LCs provides valuable insights into the phase behaviour of LCs. This paper provides a systematic study of the fluorescence properties of LCs and the influence of their molecular shape and lateral fluorination on the photo-physical properties. The emission spectra of all

investigated LCs can be deconvoluted into two Gaussians, originating from emission contributions from monomer and excimers, respectively. For the calamitics, 5CB and 8CB, there was a steady transfer from monomer emission to predominately excimer emission as the temperature was reduced. In the isotropic phase, this monomer-to-excimer transfer is more consistent between 5CB and 8CB; however, in the LC phases the rate of transfer seem to increase slightly with increased order parameter. For the CB7CB dimer, such an increase in excimer emission is only observed upon entering the N_{TB} phase regime. This could be because of an increase in AP packing in the N_{TB} phase or since the hairpin conformation in the N_{TB} phase allows self-excimer formation. However, the latter seems unlikely based on results from previous studies.[69,70,76] Reducing AP interactions by fluorination in F-CB7CB, resulted in a reduction in excimer emission by $\sim 100\times$, demonstrating that in CB-based LCs, AP interactions are key mechanisms for excimer formation and emission. For VBG93, the ratio of excimer-to-monomer emission is not affected by the LC phase and stays ~ 1 for the entire temperature range. It is possible that the excimer form of VBG93 is too difficult to form regardless of the phase due to the orientation of the overall dipole moment. The overall fluorescence of VBG93 shows a change in the gradient for emission intensity around the same temperature at which a change in the smectic layer period increases. This could be explained as an increase in disorder and out-of-plane rotations due to the increased layer spacing across this temperature region.

Conflicts of interest

There are no conflicts to declare.

Data availability

Supplementary information (SI) is available. See DOI: https://doi.org/10.1039/d5sm01147g.

The data in this paper are available in the Leeds University Data Repository (https://doi.org/10.5518/1745).

Acknowledgements

J. H., J. M. and M. N. thanks the Engineering and Physical Sciences Research Council (EPSRC) funded Centre for Doctoral Training in Soft Matter and Functional Interfaces (grant EP/L015536/1). R. J. M. thanks UKRI for funding *via* a Future Leaders Fellowship (grant MR/W006391/1) and the University of Leeds for funding *via* a University Academic Fellowship.

References

1 M. Bertolotti, G. Sansoni and F. Scudieri, *Appl. Opt.*, 1979, **18**, 528–531.
2 J. Mysliwiec, A. Szukalska, A. Szukalski and L. Sznitko, *Nanophotonics*, 2021, **10**, 2309–2346.
3 M. Grell, D. D. C. Bradley, M. Inbasekaran and E. P. Woo, *Adv. Mater.*, 1997, **9**, 798–802.
4 M. Grell and D. D. C. Bradley, *Adv. Mater.*, 1999, **11**, 895–905.
5 R. van Ewyk, I. O'Connor, A. Mosley, A. Cuddy, C. Hilsum, C. Blackburn, J. Griffiths and F. Jones, *Displays*, 1986, **7**, 155–160.
6 M. O'Neill and S. Kelly, *Adv. Mater.*, 2003, **15**, 1135–1146.
7 J. De, M. M. Abdul Haseeb, R. A. K. Yadav, S. P. Gupta, I. Bala, P. Chawla, K. K. Kesavan, J.-H. Jou and S. K. Pal, *Chem. Commun.*, 2020, **56**, 14279–14282.
8 X. Tong, Y. Zhao, B.-K. An and S. Y. Park, *Adv. Funct. Mater.*, 2006, **16**, 1799–1804.
9 A. Bobrovsky, V. Shibaev, V. Hamplová, V. Novotna and M. Kašpar, *RSC Adv.*, 2015, **5**, 56891–56895.
10 L. Zhang, Y. Cui, Q. Wang, H. Zhou, H. Wang, Y. Li, Z. Yang, H. Cao, D. Wang and W. He, *Molecules*, 2022, **27**, 5536.
11 S. Sergeyev, W. Pisula and Y. H. Geerts, *Chem. Soc. Rev.*, 2007, **36**, 1902–1929.
12 J. B. Birks, *Rep. Prog. Phys.*, 1975, **38**, 903–974.
13 J. Hobbs, J. Mattsson and M. Nagaraj, *Crystals*, 2024, **14**, 362.
14 J. Birks and L. Christophorou, *Spectrochim. Acta*, 1963, **19**, 401–410.
15 J. B. Birks, L. G. Christophorou and B. H. Flowers, *Proc. R. Soc. London, Ser. A*, 1964, **277**, 571–582.
16 E. A. Chandross and C. J. Dempster, *J. Am. Chem. Soc.*, 1970, **92**, 3586–3593.
17 J. Voskuhl and M. Giese, *Aggregate*, 2022, **3**, e124.
18 M. R. Eftink, in *Topics in Fluorescence Spectroscopy: Principles*, ed. J. R. Lakowicz, Springer US, 2002, ch. 2, pp. 53–126.
19 *Principles of Fluorescence Spectroscopy*, ed. J. R. Lakowicz, Springer US, Boston, MA, 3rd edn, 2006, pp. 277–330.
20 R. Delmdahl and R. Pätzel, *J. Phys. D: Appl. Phys.*, 2013, **47**, 034004.
21 J. B. Birks, M. D. Lumb, I. H. Munro and B. H. Flowers, *Proc. R. Soc. London, Ser. A*, 1964, **280**, 289–297.
22 R. Subramanian, L. Patterson and H. Levanon, *Chem. Phys. Lett.*, 1982, **93**, 578–581.
23 N. Tamai, I. Yamazaki, H. Masuhara and N. Mataga, *Chem. Phys. Lett.*, 1984, **104**, 485–488.
24 T. Ikeda, S. Kurihara and S. Tazuke, *J. Phys. Chem.*, 1990, **94**, 6550–6555.
25 T. Ikeda, S. Kurihara and S. Tazuke, *Liq. Cryst.*, 1990, **7**, 749–752.
26 A. Klock, W. Rettig, J. Hofkens, M. van Damme and F. De Schryver, *J. Photochem. Photobiol., A*, 1995, **85**, 11–21.
27 K. Abe, A. Usami, K. Ishida, Y. Fukushima and T. Shigenari, *J. Korean Phys. Soc.*, 2005, **46**, 220–223.
28 T. Bezrodna, V. Melnyk, V. Vorobjev and G. Puchkovska, *J. Lumin.*, 2010, **130**, 1134–1141.
29 G. V. Klishevich, N. D. Kurmei, V. I. Melnik and A. G. Tereshchenko, *J. Appl. Spectrosc.*, 2018, **85**, 904–908.
30 S. A. Oladepo, *J. Mol. Liq.*, 2021, **323**, 114590.
31 L. Dalmolen, S. Picken, A. de Jong and W. de Jeu, *J. Phys.*, 1985, **46**, 1443–1449.
32 D. G. McDonnell, E. P. Raynes and R. A. Smith, *Liq. Cryst.*, 1989, **6**, 515–523.

33 A. J. Leadbetter, J. C. Frost, J. P. Gaughan, G. W. Gray and A. Mosley, *J. Phys.*, 1979, **40**, 375–380.
34 P. E. Cladis, D. Guillon, F. R. Bouchet and P. L. Finn, *Phys. Rev. A:At., Mol., Opt. Phys.*, 1981, **23**, 2594–2601.
35 J. W. Goodby, E. J. Davis, R. J. Mandle and S. J. Cowling, *Isr. J. Chem.*, 2012, **52**, 863–880.
36 R. Dabrowski, *Liq. Cryst.*, 2015, **42**, 783–818.
37 H. F. Gleeson, S. Kaur, V. Görtz, A. Belaissaoui, S. Cowling and J. W. Goodby, *ChemPhysChem*, 2014, **15**, 1251–1260.
38 A. Jákli, O. D. Lavrentovich and J. V. Selinger, *Rev. Mod. Phys.*, 2018, **90**, 045004.
39 C. T. Imrie, R. Walker, J. M. D. Storey, E. Gorecka and D. Pociecha, *Crystals*, 2022, **12**, 1245.
40 A. Ožegovic, J. Hobbs, R. Mandle, A. Lesac and A. Kneževic, *J. Mater. Chem. C*, 2024, **12**, 13985–13993.
41 M. Martínez-Abadía, S. Varghese, B. Milián-Medina, J. Gierschner, R. Giménez and M. B. Ros, *Phys. Chem. Chem. Phys.*, 2015, **17**, 11715–11724.
42 M. Martínez-Abadía, B. Robles-Hernández, B. Villacampa, M. R. de la Fuente, R. Giménez and M. B. Ros, *J. Mater. Chem. C*, 2015, **3**, 3038–3048.
43 Y. S. K. Reddy, N. P. Lobo, S. Sampath and T. Narasimhaswamy, *J. Phys. Chem. C*, 2016, **120**, 17960–17971.
44 J. Matraszek, K. Grzeskiewicz, E. Górecka and D. Pociecha, *Liq. Cryst.*, 2020, **47**, 1803–1810.
45 M. Salamonczyk, A. Kovarova, J. Svoboda, D. Pociecha and E. Gorecka, *Appl. Phys. Lett.*, 2009, **95**, 171901.
46 R. Walker, M. Majewska, D. Pociecha, A. Makal, J. M. Storey, E. Gorecka and C. T. Imrie, *ChemPhysChem*, 2021, **22**, 461–470.
47 G. W. Gray, M. Hird, A. D. Ifill, W. E. Smith and K. J. Toyne, *Liq. Cryst.*, 1995, **19**, 77–83.
48 V. Görtz and J. W. Goodby, *Chem. Commun.*, 2005, 3262–3264.
49 J. Kimball, J. Chavez, L. Ceresa, E. Kitchner, Z. Nurekeyev, H. Doan, M. Szabelski, J. Borejdo, I. Gryczynski and Z. Gryczynski, *Methods Appl. Fluoresc.*, 2020, **8**, 033002.
50 L. Ceresa, J. Kimball, J. Chavez, E. Kitchner, Z. Nurekeyev, H. Doan, J. Borejdo, I. Gryczynski and Z. Gryczynski, *Methods Appl. Fluoresc.*, 2021, **9**, 035005.
51 N. A. Nemkovich, A. N. Rubinov and V. I. Tomin, *Topics in Fluorescence Spectroscopy: Principles*, Springer US, Boston, MA, 2002, pp. 367–428.
52 J. Mooney and P. Kambhampati, *J. Phys. Chem. Lett.*, 2013, **4**, 3316–3318.
53 J. Mooney and P. Kambhampati, *J. Phys. Chem. Lett.*, 2014, **5**, 3497.
54 B. Valeur and M. Berberan-Santos, *Molecular Fluorescence*, John Wiley & Sons, Ltd, 2nd edn, 2012, ch. 3, pp. 53–74.
55 J. R. Lakowicz, *Principles of Fluorescence Spectroscopy*, Springer US, Boston, MA, 3rd edn, 2006, ch. 10, pp. 353–382.
56 J. R. Lakowicz, *Principles of Fluorescence Spectroscopy*, Springer US, Boston, MA, 3rd edn, 2006, ch. 12, pp. 413–442.
57 B. Valeur and M. Berberan-Santos, *Molecular Fluorescence*, John Wiley & Sons, Ltd, 2nd edn, 2012, ch. 9, pp. 263–283.
58 R. G. Horn, *J. Phys.*, 1978, **39**, 105–109.
59 M. F. Palermo, A. Pizzirusso, L. Muccioli and C. Zannoni, *J. Chem. Phys.*, 2013, **138**, 204901.
60 H. Hakemi, *Liq. Cryst.*, 1989, **5**, 327–339.
61 M. Bevilacqua, A. Rinnan and M. N. Lund, *J. Chemom.*, 2020, **34**, e3286.
62 F. Schneider, *Phys. Rev. E:Stat., Nonlinear, Soft Matter Phys.*, 2006, **74**, 021709.
63 S. Sharafy and K. A. Muszkat, *J. Am. Chem. Soc.*, 1971, **93**, 4119–4125.
64 R. J. Mandle and J. W. Goodby, *Phys. Chem. Chem. Phys.*, 2019, **21**, 6839–6843.
65 P. Kubala, W. Tomczyk and M. Ciesla, *J. Mol. Liq.*, 2022, 120156.
66 E. J. Bowen and J. Sahu, *J. Phys. Chem.*, 1959, **63**, 4–7.
67 E. E. Zavvou, E. Ramou, Z. Ahmed, C. Welch, G. H. Mehl, A. G. Vanakaras and P. K. Karahaliou, *Soft Matter*, 2023, **19**, 9224–9238.
68 M. R. Tuchband, M. Shuai, K. A. Graber, D. Chen, C. Zhu, L. Radzihovsky, A. Klittnick, L. Foley, A. Scarbrough, J. H. Porada, M. Moran, J. Yelk, J. B. Hooper, X. Wei, D. Bedrov, C. Wang, E. Korblova, D. M. Walba, A. Hexemer, J. E. Maclennan, M. A. Glaser and N. A. Clark, *Crystals*, 2024, **14**, 583.
69 A. Kocot, B. Loska, Y. Arakawa and K. Merkel, *Phys. Rev. E*, 2022, **105**, 044701.
70 K. Merkel, B. Loska, Y. Arakawa, G. H. Mehl, J. Karcz and A. Kocot, *Int. J. Mol. Sci.*, 2022, **23**, 11018.
71 D. A. Paterson, M. Gao, Y.-K. Kim, A. Jamali, K. L. Finley, B. Robles-Hernández, S. Diez-Berart, J. Salud, M. R. de la Fuente, B. A. Timimi, H. Zimmermann, C. Greco, A. Ferrarini, J. M. D. Storey, D. O. López, O. D. Lavrentovich, G. R. Luckhurst and C. T. Imrie, *Soft Matter*, 2016, **12**, 6827–6840.
72 G. Babakhanova, Z. Parsouzi, S. Paladugu, H. Wang, Y. A. Nastishin, S. V. Shiyanovskii, S. Sprunt and O. D. Lavrentovich, *Phys. Rev. E*, 2017, **96**, 062704.
73 M. Cestari, S. Diez-Berart, D. A. Dunmur, A. Ferrarini, M. R. de la Fuente, D. J. B. Jackson, D. O. Lopez, G. R. Luckhurst, M. A. Perez-Jubindo, R. M. Richardson, J. Salud, B. A. Timimi and H. Zimmermann, *Phys. Rev. E:Stat., Nonlinear, Soft Matter Phys.*, 2011, **84**, 031704.
74 K. Sasaki, M. Nagasaka and Y. Kuroda, *Chem. Commun.*, 2001, 2630–2631.
75 D. W. Cho, M. Fujitsuka, A. Sugimoto and T. Majima, *J. Phys. Chem. A*, 2008, **112**, 7208–7213.
76 G. Yu and M. R. Wilson, *Soft Matter*, 2022, **18**, 3087–3096.
77 B. Strehmel, A. M. Sarker, J. H. Malpert, V. Strehmel, H. Seifert and D. C. Neckers, *J. Am. Chem. Soc.*, 1999, **121**, 1226–1236.
78 M. Piacenza, F. Della Sala, G. M. Farinola, C. Martinelli and G. Gigli, *J. Phys. Chem. B*, 2008, **112**, 2996–3004.
79 M. Piacenza, D. Comoretto, M. Burger, V. Morandi, F. Marabelli, C. Martinelli, G. M. Farinola, A. Cardone, G. Gigli and F. Della Sala, *ChemPhysChem*, 2009, **10**, 1284–1290.

80 B. Milián-Medina, S. Varghese, R. Ragni, H. Boerner, E. Ortí, G. M. Farinola and J. Gierschner, *J. Chem. Phys.*, 2011, **135**, 124509.
81 R. Milad, J. Shi, A. Aguirre, A. Cardone, B. Milián-Medina, G. M. Farinola, M. Abderrabba and J. Gierschner, *J. Mater. Chem. C*, 2016, **4**, 6900–6906.
82 M. Hird and K. J. Toyne, *Mol. Cryst. Liq. Cryst. Sci. Technol., Sect. A*, 1998, **323**, 1–67.
83 M. Nagaraj, J. C. Jones, V. P. Panov, H. Liu, G. Portale, W. Bras and H. F. Gleeson, *Phys. Rev. E:Stat., Nonlinear, Soft Matter Phys.*, 2015, **91**, 042504.
84 M. Nagaraj, *Liq. Cryst.*, 2016, **43**, 2244–2253.
85 L. E. Hough, M. Spannuth, M. Nakata, D. A. Coleman, C. D. Jones, G. Dantlgraber, C. Tschierske, J. Watanabe, E. Körblova, D. M. Walba, J. E. Maclennan, M. A. Glaser and N. A. Clark, *Science*, 2009, **325**, 452–456.
86 L. van't Hag, S. L. Gras, C. E. Conn and C. J. Drummond, *Chem. Soc. Rev.*, 2017, **46**, 2705–2731.
87 M. Kasha, H. R. Rawls and M. A. El-Bayoumi, *Pure Appl. Chem.*, 1965, **11**, 371–392.
88 T. Förster, *J. Biomed. Opt.*, 2012, **17**, 011002.
89 U. Rösch, S. Yao, R. Wortmann and F. Würthner, *Angew. Chem., Int. Ed.*, 2006, **45**, 7026–7030.
90 M. Cigán, J. Donovalová, V. Szöcs, J. Gašpar, K. Jakusová and A. Gáplovský, *J. Phys. Chem. A*, 2013, **117**, 4870–4883.
91 N. H. Mudliar and P. K. Singh, *Chem. – Eur. J.*, 2016, **22**, 7394–7398.
92 H. Kresse, in *Advances in Liquid Crystals*, ed. G. H. Brown, Elsevier, 1983, vol. 6, pp. 109–172.
93 Q. Liao, S. Aya and M. Huang, *Liq. Cryst. Rev.*, 2024, **12**, 149–194.
94 R. J. Mandle, N. Sebastián, J. Martinez-Perdiguero and A. Mertelj, *Nat. Commun.*, 2021, **12**, 4962.
95 N. V. Madhusudana, *Phys. Rev. E*, 2021, **104**, 014704.
96 C. J. Gibb, J. Hobbs and R. J. Mandle, *J. Am. Chem. Soc.*, 2025, **147**, 4571–4577.

